BULLETIN OF THE POLISH ACADEMY OF SCIENCES
TECHNICAL SCIENCES, Vol. 74(5), 2026, Article number: 1622
DOI: 10.24425/bpasts.2026.1622

Soft-switching of IGCTs in three-level voltage source inverter

Zbigniew SZULAR* and **Witold MAZGAJ**

Cracow University of Technology, Warszawska 24, 31-155 Kraków, Poland

Abstract. This paper presents a soft-switching system in three-level voltage source inverters based on Integrated Gate-Commutated Thyristors. The proposed soft-switching system refers to inverter thyristors connected to the voltage source terminals. The operation principles of the inverter equipped with the proposed soft-switching solution are discussed in detail herein. The main thyristors are controlled in the same manner as those in an inverter operating with a hard-switching technique. The correctness of the IGCT model used in the calculations is verified by comparing numerically obtained voltage and current with waveforms recorded at the laboratory stand. Numerical analysis is performed for the voltage source inverter of the rated power of 10 MW (2×2.5 kV, 3.0 kA). Examples of voltage and current waveforms for a single switching of one of the main thyristors and selected waveforms for two periods of the inverter output voltage are presented. The switching losses of the three-level voltage source inverter with the described soft-switching system are compared with those in an inverter with the hard-switching technique. The proposed soft-switching solution allows for increasing inverter efficiency.

Keywords: integrated gate-commutated thyristor; soft-switching; switching losses; three-level voltage source inverter.

1. INTRODUCTION

Integrated Gate-Commutated Thyristors (IGCTs) are fully controlled elements with the highest unit powers [1–13]. Their gate circuits are integrated with semiconductor structures; this allows for reducing the influence of parasitic inductance. Additionally, the voltage drop in conduction states is lower in comparison to Insulated Gate Bipolar Transistors (IGBTs) [6, 14, 15]. At present, their maximum rated voltage and current are about 6.5 kV and 4 kA, respectively. These elements are mainly used in multi-level converters [4, 16], especially in three-level voltage source inverters (3LVSIs), which are often applied in high-power drives and in energy conversion systems from renewable sources [1, 2, 17–19]. Since the switching times of IGCTs are in the order of several microseconds, multi-level inverters allow limiting the content of higher harmonics at a relatively low switching frequency. The IGCTs are also applied in DC circuit breakers instead of electromagnetic switches [20, 21]. Research focuses on the use of these thyristors in DC-DC resonant converters and High Voltage DC systems [22–26], as well as on failure states in modular multilevel converters based on IGCTs [27, 28].

Unlike IGBTs, IGCTs are current-controlled. They are turned ON with a relatively small current signal. However, to turn them OFF, a large current, which should even be equal to the rated current of the tested thyristor, must flow through the gate-cathode circuit during several microseconds. Therefore, IGCT controllers have a complex structure. During their turn-ON processes, the current derivative di/dt cannot be higher than the value given in datasheets. A similar condition applies to the thyristor voltage derivative dv/dt in the blocking state.

The total losses in IGCTs are a sum of both the conduction and switching losses. Users of the power electronics devices do not have influence on the first kind of losses because they depend on the state-ON voltage across the given IGCT. The main switching losses in the IGCTs occur during the turn-OFF processes, and they are about ten times higher than losses occurring in turn-ON processes. Note that the turn-OFF process of IGCTs is extraordinarily complex because the negative current pulse in the gate-cathode circuit must bring the cathode current to zero [15]. Figure 1 shows simplified waveforms of the voltage and current during the turn-ON and turn-OFF processes, respectively. Notably, total switching losses in the 3LVSI (Fig. 2) operating with a hard-switching technique are increased by the losses occurring in diodes during their reverserecovery processes. However, they are relatively small, because the speed of the current rise should be reduced due to the permissible value of the thyristor current derivative di/dt. For this purpose, a snubber is used, but losses occurring in snubbers amount to a few percent of the total power losses.

The turn-OFF losses can be reduced when the voltage across the thyristor equals almost zero during the turn-OFF process. The scientific literature contains individual suggestions for such a system; however, they concern relatively simple converters with IGCTs [23, 29].

The papers [30, 31] present results of research on possibilities of turning OFF when the voltage between the anode and the cathode of the IGCT is reduced. The results demonstrate that at a voltage close to zero, the IGCT can turn OFF a significantly higher current than its rated value. It is advisable that during

*e-mail: zbigniew.szular@pk.edu.pl

Manuscript submitted 2026-02-12, revised 2026-05-20, initially accepted for publication 2026-06-03, published in September 2026.

© 2026 The Author(s). This is an open access article under the CC BY license (http://creativecommons.org/licenses/by/4.0/)

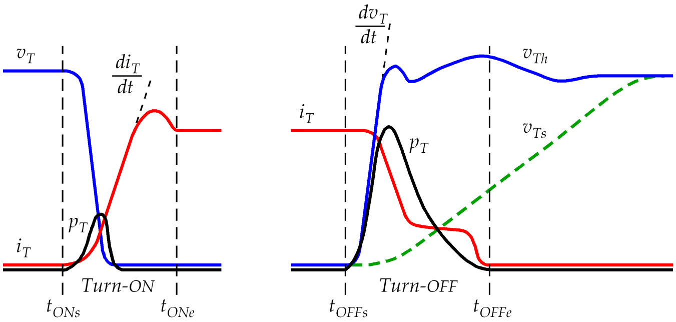

Fig. 1. Simplified waveforms of the IGCT during switching processes: v_{Th}, i_T – voltage and current of the IGCT during a hard turn-OFF process, respectively; v_{Ts} – expected voltage of the IGCT during a soft turn-OFF process; di_T/dt – derivative of the IGCT current; dv_T/dt – derivative of the IGCT voltage; t_{ONs}, t_{ONe}, t_{OFFs}, t_{OFFe} – start and end of the turn-ON and turn-OFF processes of IGCT, respectively

the turn-OFF process of the IGCT, its voltage should be close to zero, as indicated by the dashed line in Fig. 1.

This paper aims to propose a soft-switching system in the 3LVSI based on IGCTs. It was assumed that the basic control algorithm applied in the 3LVSI with the hard-switching technique remains unchanged. The new feature is the modified topology of the 3LVSI with additional circuits that limit the voltage rise during the turn-OFF process of the IGCTs.

The inductors Lsp and Lsn limit the current rise rate in the IGCTs, so that the derivative di_T/dt (specified in datasheets) is not exceeded. Diodes Dsp, Dsn, resistors Rsp, Rsn and capacitors Csp, Csn are used to dissipate the energy of the magnetic field of inductors Lsp and Lsn after the IGCT is turned OFF. Each IGCT has individual protection as a series-connected capacitor and resistor (not marked in Fig. 2) against too sudden increase in the blocking voltage.

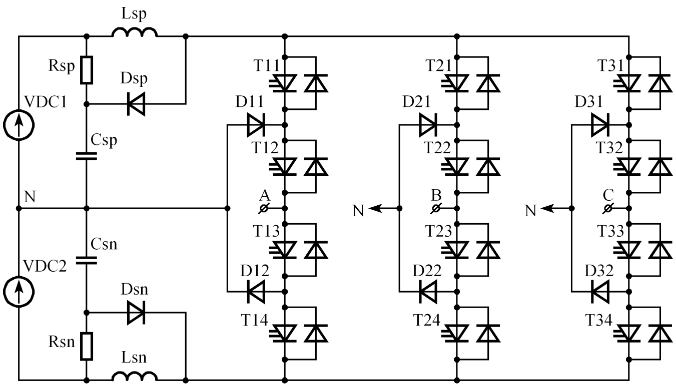

Fig. 2. Three-level voltage source inverter (3LVSI) with the hard-switching technique: A, B, C – load terminals; N – neutral point

The principles of the inverter control are shown in Fig. 3. Two sawtooth waveforms v_p and v_n are compared to the reference waveform v_{ref}. If values of the v_{ref} are greater than the corresponding values v_p, thyristor T11 (in the first phase) is turned ON. Thyristor T14 is turned ON when values of the v_{ref} are lower than the values of the sawtooth waveform v_n.

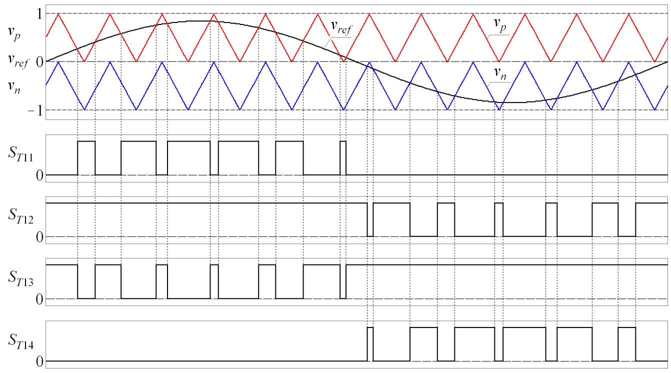

Fig. 3. Control principle of the three-level voltage source inverter: v_p, v_n – sawtooth waveforms, v_{ref} – reference waveform, $S_{\text{T11-14}}$ – control signals of thyristors T11–T14

Thyristors T12 and T13 are controlled by the negated signal of the thyristors T14 and T11, respectively. It means that at high load current values, the IGCTs T11 and T14, connected directly to the voltage source terminals, are turned ON and OFF, and the main thyristors T12 and T13, connected to the load terminals, are either turned ON or OFF depending on the operating state of T11 and T14.

The structure and operating principles of the 3LVSI with the proposed soft-switching system are described in Section 2. This section includes simplified waveforms of chosen voltages and currents and describes individual stages of the inverter operation. The selection of the thyristors and passive components is presented in Section 3. The next section refers to the IGCT model. To verify this model, the measured waveforms of both the thyristor current and voltage are compared with analogous numerically determined waveforms. Section 5 discusses the power losses in the 3LVSI with the soft-switching system. They are compared with those in the inverter with the hard-switching technique.

2. SOFT-SWITCHING SYSTEM IN THREE-LEVEL VOLTAGE SOURCE INVERTER

2.1. Structure and work principles

The structure of the 3LVSI with the proposed soft-switching system is shown in Fig. 4 [32]. Both voltage sources, VDC1 and VDC2, set the same voltage V_{DC}. Capacitors C11 and C14 (in the first phase of the 3LVSI) are applied to decrease the steepness of the voltage increase of the main IGCTs T11 and T14 during their turn-OFF processes. The use of inductors L11 and L14 is intended to reduce the rate of the current rise of IGCTs during their turn-ON processes, so that the thyristor current derivative does not exceed the permissible value given in datasheets. These inductors have a significant impact on the voltage increase on the IGCTs during their turn-OFF processes. The inductors L12 and L13 are used to limit the derivative di/dt when the IGCTs T12 and T13 are turned ON. Thyristors T11a and T14a are auxiliary fast thyristors that turn OFF themselves when their currents decrease to zero. Both the IGCTs and auxiliary fast thyristors have protection systems against a sudden increase in the blocking voltage (dashed circuits in Fig. 4).

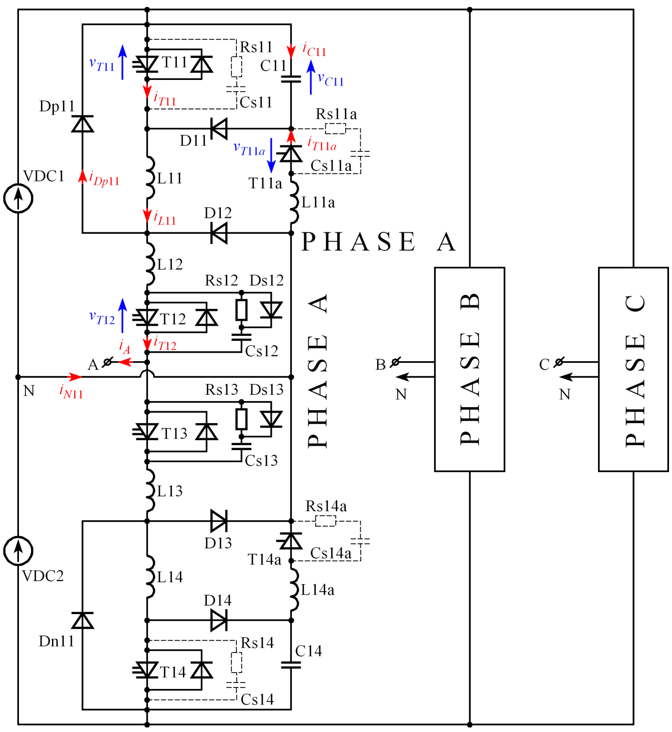

Fig. 4. Three-phase 3LVSI with the proposed soft-switching system; dashed lines refer to RC circuits that protect against overvoltages

The analysis of the inverter operation is conducted for the case when thyristor T11 is switched, and T12 is still turned ON. The inverter operation is described for one switching cycle.

2.2. Working stages

Simplified selected waveforms, when thyristor T11 is switched, and T12 conducts continuously, are shown in Fig. 5. The circuits (with marked currents) corresponding to individual time intervals are shown in Fig. 6.

Figure 7 shows the operating stages for the opposite direction of the load current of the phase A relative to the direction marked in Fig. 6.

Before time t_{11}, the main thyristor T11 is in a conduction state, and the load current i_A, which in the further part of the article is marked as I_L, flows from VDC1 through thyristor T11, inductors L11, L12, and thyristor T12 to the load phase A (Fig. 6a). It was assumed that the current I_L does not change its value in the analyzed stages. The capacitor C11 is completely discharged.

Stage t_{11}–t_{12}, Fig. 6b

The main thyristor T11 is turned OFF at time t_{11}. The current I_L begins to flow through capacitor C11 and diode D11. The voltage across the main thyristor T11 increases linearly with time. This allows us to conclude that the turn-OFF process of the thyristor T11 is soft. The rate of the voltage increase on the capacitor C11, and thus the voltage on the thyristor T11, has a decisive influence on the losses occurring during the turn-OFF processes. The voltage of thyristor T11 changes as follows

$$v_{\mathrm{T11}}(t) = v_{\mathrm{C11}}(t) = \frac{I_L(n)}{C_{11}} t, \tag{1}$$

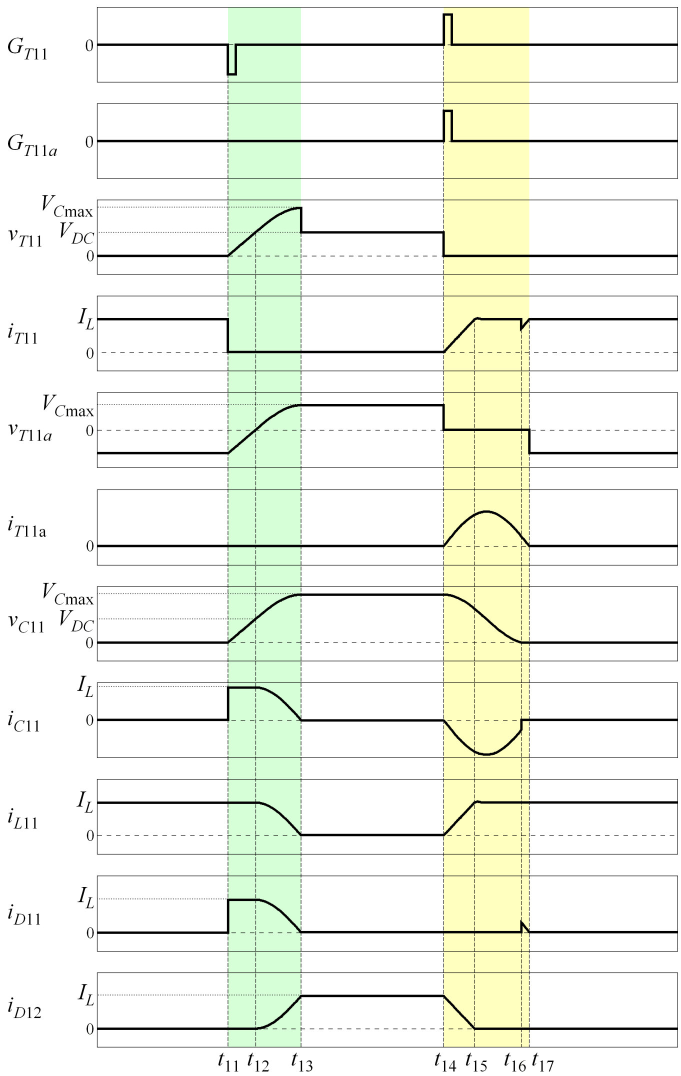

Fig. 5. Simplified waveforms when T11 is switched: v_{GT11}, v_{GT11a} – control signals of thyristors T11 and T11a, respectively; v_{T11}, i_{T11} – voltage and current of thyristor T11, respectively; v_{T11a}, i_{T11a} – voltage and current of thyristor T11a; v_{C11}, i_{C11} – voltage and current of capacitor C11, respectively; i_{L11} – current of inductor L11; i_{D11}, i_{D12} – current of diodes D11 and D12, respectively; I_L – load current; green and yellow colors – processes related to the turn-OFF and turn-ON of IGCT, respectively

where $v_{C11}(t_{11}) = 0$, n denotes a certain switching cycle, $I_L(n)$ is the current in n-th cycle.

Stage t_{12}–t_{13}, Fig. 6c

From time t_{12}, the current flowing through capacitor C11 decreases. At the same time, a current from the voltage source VDC2 (point N) begins to flow through diode D12. The capacitor C11 is resonantly charged to a voltage higher than V_{DC}. Changes in the capacitor voltage can be determined using equation

$$C_{11} L_{11} \frac{d^2 v_{\mathrm{C11}}(t)}{dt^2} + v_{\mathrm{C11}}(t) = V_{\mathrm{DC1}}, \tag{2}$$

where $v_{\mathrm{C11}}(t_{12}) = V_{\mathrm{DC1}}$, and $i_{\mathrm{L11}}(t_{12}) = I_L(n)$.

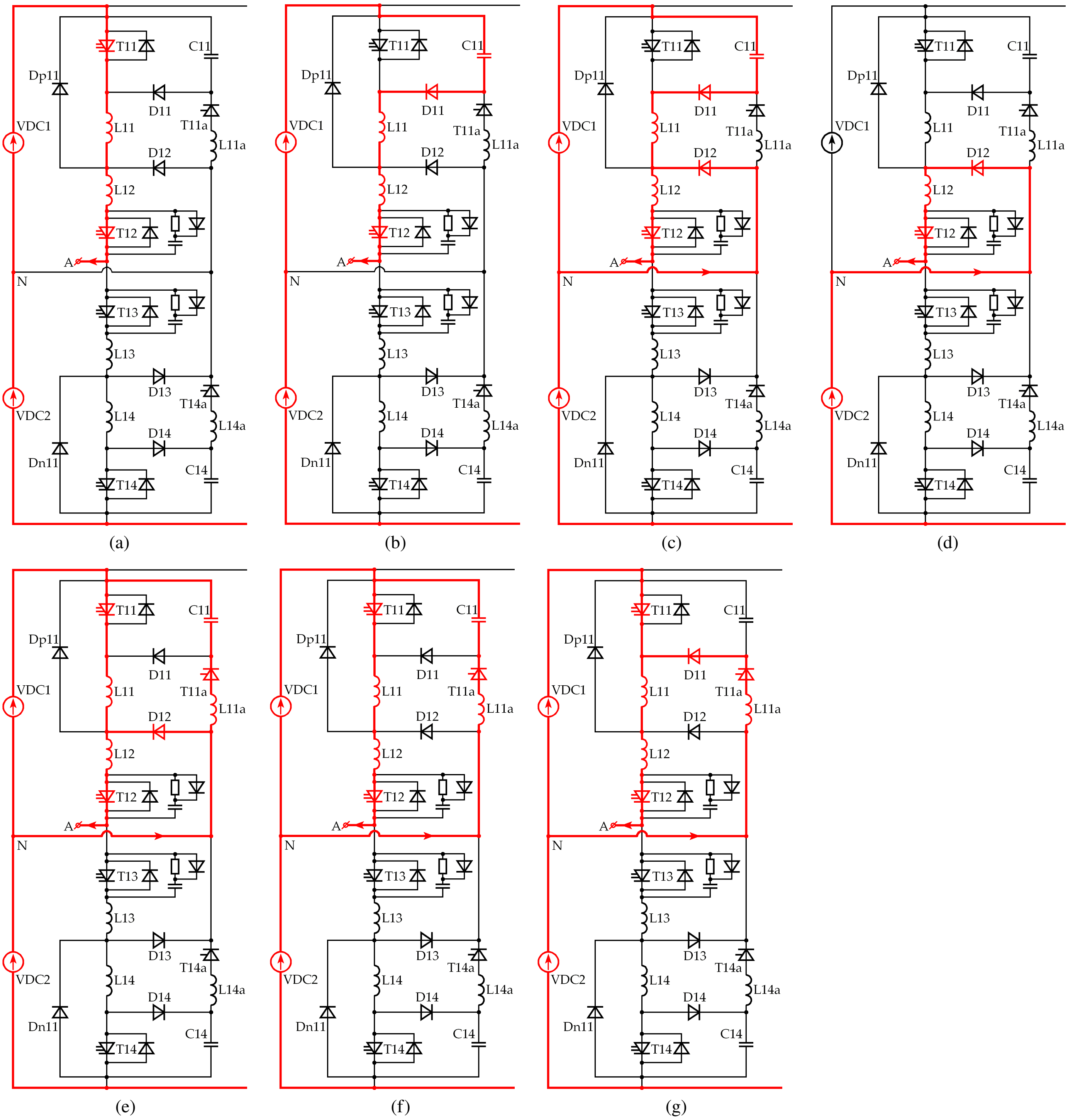

Fig. 6. Operation stages when thyristor T11 is switched

Assuming $V_{DC1} = V_{DC2} = V_{DC}$, the following formulas determine the capacitor voltage and current

$$v_{C11}(t) = V_{DC} + \sqrt{\frac{L_{11}}{C_{11}}} I_L(n) \sin\left(\frac{t}{\sqrt{C_{11}L_{11}}}\right), \tag{3}$$

$$i_{C11}(t) = I_L(n) \cos\left(\frac{t}{\sqrt{C_{11}L_{11}}}\right), \tag{4}$$

The maximum capacitor voltage is

$$V_{C11\,max} = V_{DC} + \sqrt{\frac{L_{11}}{C_{11}}} I_{L\,max}, \tag{5}$$

where $I_{L\,max}$ denotes the maximum load current.

Stage t_{13}–t_{14}, Fig. 6d

In this stage, the load current I_L flows only from VDC2 through D12, L12 and T12 to the load terminal A.

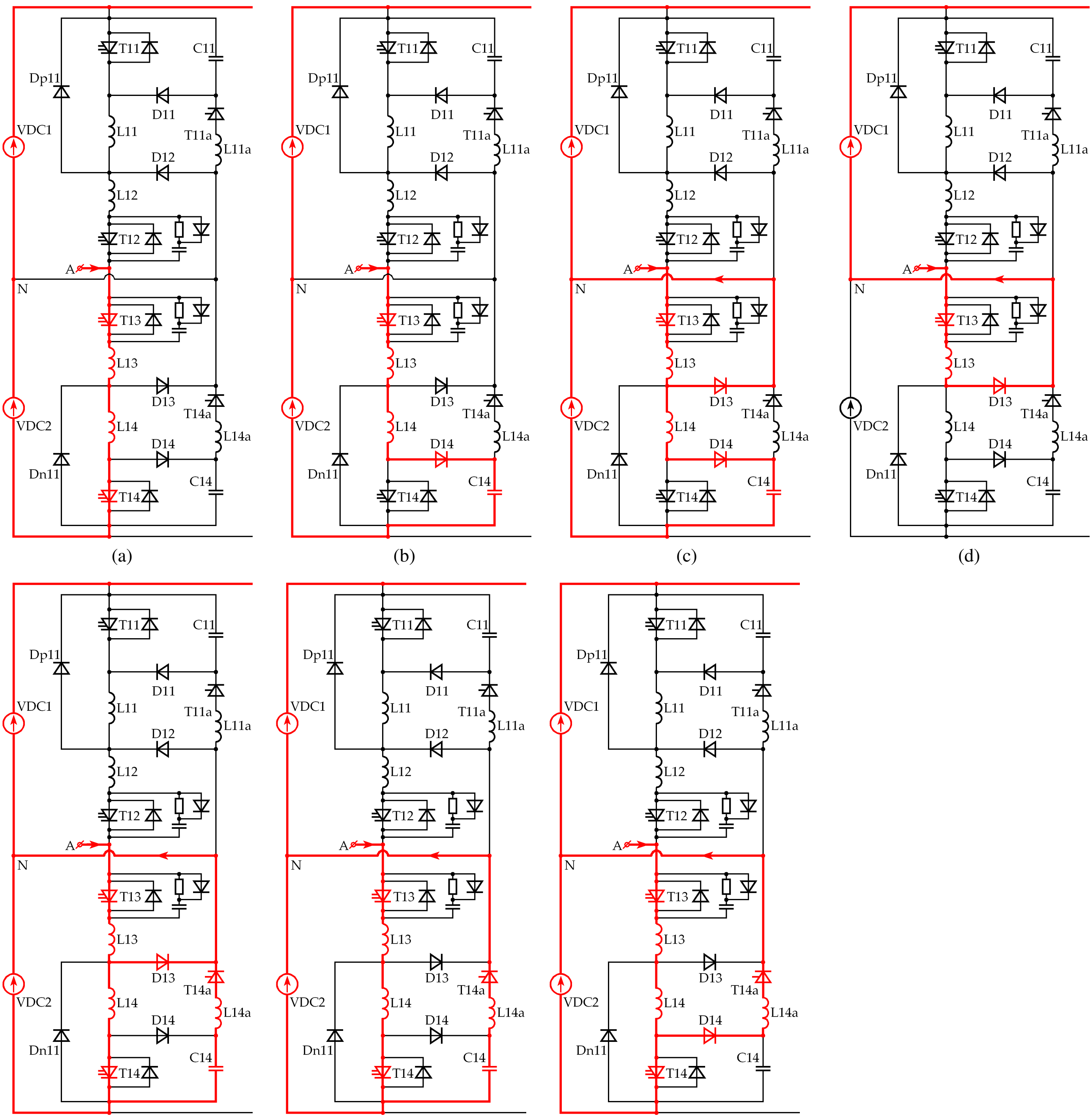

Fig. 7. Operation stages when thyristor T14 is switched

Stage t_{14}–t_{15}, Fig. 6e
At time t_{14}, the main thyristor T11 and the auxiliary thyristor T11a are turned ON. The current of thyristor T11, which is equal to the current of inductor L11, increases slowly to the current I_L, and it is described by a simple differential equation

$$L_{11}\frac{di_{\mathrm{L11}}}{dt} = V_{\mathrm{DC}}, \tag{6}$$

where $i_{\mathrm{L11}}(t_{14}) = 0$.

Hence, the current changes of the main thyristor T11 are described as follows

$$i_{\mathrm{T11}}(t) = i_{\mathrm{L11}}(t) = \frac{V_{\mathrm{DC}}}{L_{11}}t. \tag{7}$$

The inductor L11 allows to limit the rate of the current rise of thyristor T11, so that the current derivative di/dt should be not higher than the permissible value given in datasheets. The current of thyristor T11 reaches the load current value I_L at time t_{15}.

At time t_{14}, capacitor C11 begins to discharge resonantly and its current flows through the voltage source VDC1, inductor L11a and auxiliary thyristor T11a. Since the auxiliary thyristor T11a is turned ON at a current close to zero, due to the resonant nature of the current increase, the auxiliary thyristor T11a is turned ON softly. The following equation allows to determine the capacitor voltage

$$L_{11}\frac{i_{\mathrm{L11a}}(t)}{dt} - v_{\mathrm{C11}}(t) = V_{\mathrm{DC1}}, \tag{8}$$

where $i_{\mathrm{L11a}}(t_{14}) = 0$, $v_{\mathrm{C11}}(t_{14}) = V_{\mathrm{C11\,max}}$.

Assuming a certain coefficient k as $k = V_{\mathrm{C11\,max}}/V_{\mathrm{DC}}$, the maximum capacitor current is

$$I_{\mathrm{C11\,max}}(t) = (k-1)V_{\mathrm{DC}}\sqrt{\frac{C_{11}}{L_{11a}}}. \tag{9}$$

Stage t_{15}–t_{16}, Fig. 6f
The time period t_{15}–t_{16} depends on the current I_L. At time t_{15} the current of the main thyristor T11 reaches the value of the load current, and the current of diode D12 decreases to zero. Capacitor C11 is still resonantly discharging.

Stage t_{16}–t_{17}, Fig. 6g
At time t_{16}, the voltage across capacitor C11 reaches zero, which causes the current of this capacitor to decrease abruptly to zero. At this time, diode D11 may start to conduct if the current of the auxiliary inductor L11a has not yet decreased to zero before the capacitor discharge process is complete. As a result, the current of the main thyristor T11 abruptly decreases, which does not affect the correct operation of the 3LVSI with the proposed soft-switching system. In time interval t_{16}–t_{17}, the currents of the diode D11, auxiliary thyristor T11a and inductor L11a decrease linearly to zero, and the current of the main thyristor T11 increases linearly to the load current. The auxiliary thyristor T11a turns OFF automatically when its current reaches zero at time t_{17}. At this time, capacitor C11 is completely discharged, and the load current I_L flows similarly as shown in Fig. 6a. In order the next turn-OFF process of the thyristor T11 to be soft, the capacitor C11 should be completely discharged.

The thyristor T11a can be a not fully controllable "classic" thyristor because the resonant discharge process ends when the discharge current drops to zero; this causes the thyristor T11a turns OFF automatically. Thanks to this, the control system of the auxiliary thyristors becomes simpler than similar system in 3LVSI based on IGBTs [33], because thyristor T11a requires only a turn-ON pulse. Due to the nature of the resonant discharge, fast thyristors should be applied.

When the IGCT T14 is switched (Fig. 7), changes in the voltages and currents of this IGCT and capacitor C14 are described by relationships similar to (1)–(9).

2.3. Switching of thyristor T12

When describing the switching of the thyristor T12, it is assumed that this thyristor is initially turned ON, and all other thyristors in the first phase are turned OFF. The current flows from the neutral point N through D12, L12 and T12 to the load phase A (Fig. 4). At time t_{21}, thyristor T12 is turned OFF, and its current abruptly decreases to zero. The load phase current I_L flows from the neutral point N through D12, L12, Ds12 and capacitor Cs12. The components L12, Rs12, Cs12 and Ds12 protect thyristor T12 against excessive di_T/dt current derivative during its turn-ON process. At time t_{22}, the voltage across the main thyristor T12 reaches the value V_{DC}.

The main thyristor T12 is turned ON at time t_{23}. The voltage across this thyristor abruptly decreases to zero. The current of T12 reaches the load current at time t_{24}. Simplified waveforms of the voltage and current of the thyristor T12 are shown in Fig. 8. Diodes Dp11 and Dn11 conduct current during the switching of the thyristors T12 and T13. However, these diodes do not affect the operation of the soft-switching of thyristors T11 and T14.

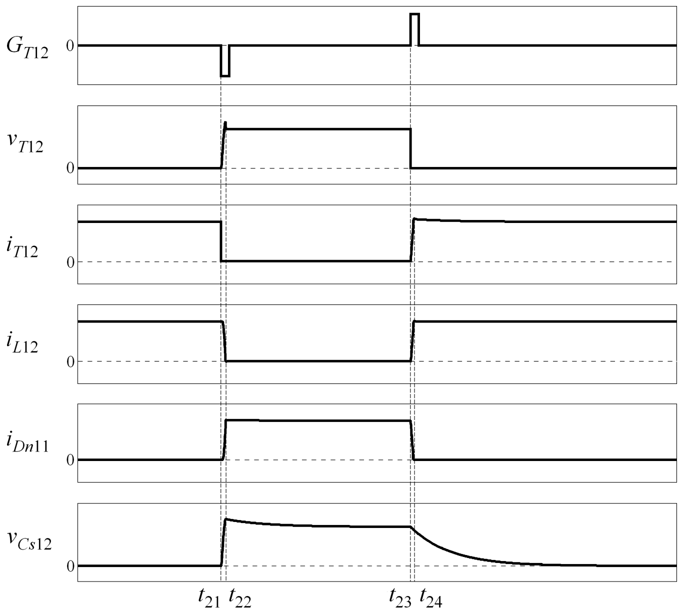

Fig. 8. Simplified waveforms when T12 is switched: G_{T12} – control signal of thyristor T12; v_{T12}, i_{T12} – voltage and current of thyristor T12, respectively; i_{L12} – current of inductor L12; i_{Dn11} – current of diode Dn11; v_{Cs12} – voltage of capacitor Cs12

2.4. Switching algorithm

The principle of the control algorithm is presented in Fig. 9, which shows the signals controlling the operation of all thyristors and the pulses turning ON and OFF, as well as pulses turning ON auxiliary fast thyristors. The thyristors T11 and T14, connected to the power supply terminals, are controlled in priority to the thyristors T12 and T13, connected to the load terminal A. The main thyristor T12 is controlled by a negated signal relative to the signal to the main thyristor T14, and thyristor T13 is controlled by a negated signal relative to T11. The main thyristor T11 is turned ON by a positive gate current pulse G_{T11} generated by control signal S_{T11} from an external, higher-level control system if the instantaneous value of the load phase current i_A is greater than a preset negative load current threshold $-I_{\mathrm{tr}}$. The thyristor T11 is turned OFF by a negative gate current pulse. If the instantaneous value of the phase current i_A is less than

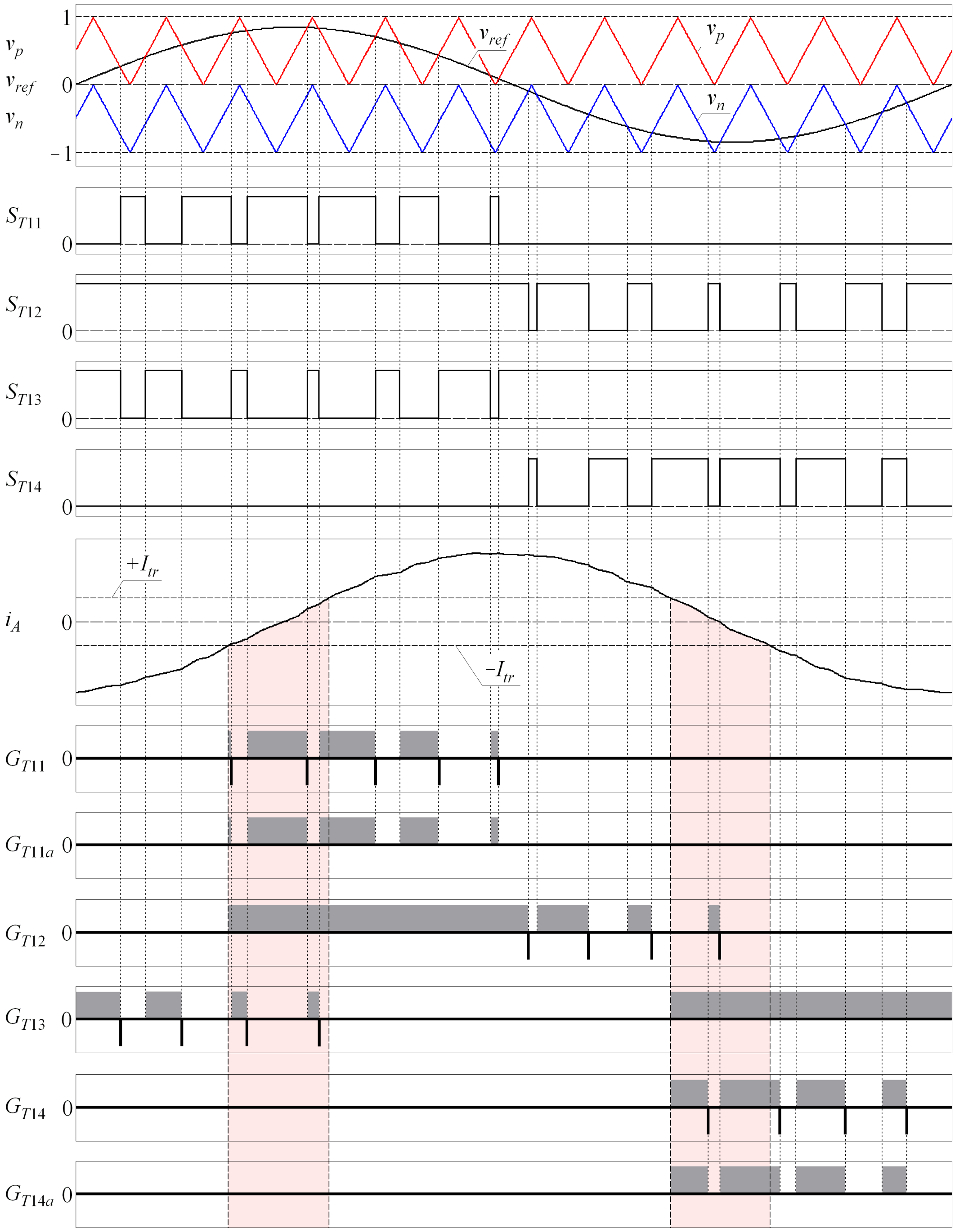

Fig. 9. Control signals and pulses turning the thyristors ON and OFF; I_{tr} – threshold value of phase current, S_{T11}, S_{T12}, S_{T13}, S_{T14} – control signals of main IGCTs, G_{T11}, G_{T12}, G_{T13}, G_{T14} – switching pulses of main IGCTs, G_{T11a}, G_{T14a} – pulses turning ON auxiliary thyristors; pink color – all IGCTs can be switched

$-I_{tr}$, thyristor T11 is not turned ON. The main thyristor T14 is turned ON by a positive gate current pulse if the instantaneous value of the load phase current i_A is less than the preset positive load current threshold $+I_{tr}$, and it is turned OFF by a negative gate current pulse. If the instantaneous value of the current i_A is greater than $+I_{tr}$, then T14 is not turned ON.

The current pulses that turn ON thyristors T12 and T13 should be sufficiently long because it is difficult to precisely determine when T12 or T13 can begin conducting the load current. If the load current i_A changes between $-I_{tr}$ and $+I_{tr}$, then thyristors T12 and T13 conduct alternately.

The auxiliary thyristors T11a and T14a are turned ON simultaneously with thyristors T11 and T14, respectively. Note that the auxiliary thyristors turn themselves OFF if their currents decrease to zero.

It should be emphasized that the basic control algorithm (e.g., sinusoidal PWM, vector control method, etc.) generating signals $S_{T11-T14}$ is the same as in an inverter with the hard-switching technique. Thyristors T11, T12, and T11a are switched when the direction of the load phase current is as shown in Fig. 6. For the opposite direction of the load current, the remaining IGCTs are switched. The purpose of the described control method is to reduce losses in the circuits with IGCTs, which do not need to be switched during individual operation stages. This reduces power losses in the inverter. The value I_{tr} should be as low as possible at the level of guaranteed detection by the measuring system. This threshold value in Fig. 9 is intentionally much higher to better illustrate the control method. In practice, this value is on the order of several percent relative to the rated load current. In the numerical calculations, the I_{tr} value was equal to 30 A.

The main thyristors T12 and T13 are hard-switched, although inductors L12 and L13 limit the current rise and capacitors Cs12 and Cs13 affect the thyristor voltage rise during its turn-OFF process. Note that these components are used to ensure that the derivatives di/dt and dv/dt do not exceed their values specified in datasheets.

3. SELECTION OF INVERTER COMPONENTS

3.1. Selection of thyristors

The IGCTs in the 3LVSI working with the hard-switching technique are selected for a single supply voltage V_{DC}. However, owing to the operation principles of the described soft-switching system, IGCTs should be selected for rated voltages at twice the supply voltage VDC, and this also refers to diodes and capacitors. This represents inconvenience for the proposed soft-switching system. The turn-OFF processes of the main IGCTs have a soft character when the maximum voltage of the capacitors is no less than twice the voltage V_{DC}. The maximum voltage of the main IGCTs, which is the same as the maximum voltage of the capacitors, is determined using equation (5).

3.2. Reactive elements

To reduce the turn-OFF losses, the key role of the capacitors is to limit the rate of the voltage rise across the main IGCT when it is turned OFF. Datasheets do not provide turn-OFF times of IGCTs. Only in some cases, the current falling time from 90% to 40% of the thyristor current during the turn-OFF is specified. However, the so-called "tail" current, which has a significant impact on turn-OFF losses, is omitted. The total turn-OFF time of IGCTs (including "tail" current) is approximately from 2 µs to 6 µs. Therefore, the capacitors are determined for several turn-OFF times, and for an assumed voltage that should not be exceeded during the turn-OFF process. Since in the initial period of the turn-OFF process the load current flows through C11, and based on equation (1), the capacitance C_{11} (C_{14} for the opposite direction of the load current) is equal to

$$C_{11} = \frac{I_{L\max}}{V_{COFF}} t_{OFF}, \tag{10}$$

where V_{COFF} denotes an assumed maximum capacitor voltage, and t_{OFF} is an assumed time of the turn-OFF process.

Despite the simplicity of equation (10), Table 1 shows the capacitor capacitance for assumed values of the IGCT turn-OFF duration for two V_{COFF} voltages.

Table 1
Capacitance in µF for $I_{L\max} = 3.0$ kA, $V_{DC} = 2.5$ kV

t_{OFF} (µs)	2.0	4.0	6.0	8.0
$V_{COFF} = 0.1V_{DC}$	24	48	72	96
$V_{COFF} = 0.2V_{DC}$	12	24	36	48

The key role of inductors L11 and L14 is to limit the current rise during turn-ON processes. Assuming that all inductors that are connected with the thyristors T11 and T14 have the same L_m inductances, and based on equation (6), it can be written as

$$\frac{di_T}{dt} = \frac{V_{DC}}{L_m} \leq \left.\frac{di}{dt}\right|_{cr}. \tag{11}$$

Hence, inductance L_m is equal

$$L_m = \frac{V_{DC}}{\left.\frac{di}{dt}\right|_{cr}}. \tag{12}$$

The turn-OFF process of the main thyristors is soft if the capacitor is completely discharged when this process begins. Hence, the voltage $V_{C\max}$ should be at least $2V_{DC}$. If the voltage $V_{C\max}$ is less than twice the V_{DC} voltage value, then based on equation (5), the inductance L_m should be increased

$$L_m = C_{11} \frac{V_{DC}^2}{I_{L\max}^2}. \tag{13}$$

When determining the inductance L_m, a higher value should be selected based on equations (12) and (13). Note that increasing the inductance L_m causes the rise time of the capacitor voltage to be longer, which may affect the selection of the switching frequency.

The admissible value of the current derivative should also be taken into consideration when selecting the auxiliary fast thyristors. The derivative of the current of the auxiliary thyristor in the initial stage of the discharge process of capacitors is equal to

$$\frac{di_{Ta}}{dt} = \frac{V_{DC}}{L_a}, \tag{14}$$

where L_a is the inductance of the inductors connected in series with the auxiliary thyristors.

The inductors L11a and L14a limit the maximum resonant discharge current of the capacitors. Based on equation (9), their inductance L_a is

$$L_a = (V_{C\max} - V_{DC})^2 \frac{V_{DC}}{I_{C\max}^2}, \tag{15}$$

where $I_{C\max}$ denotes the maximum current of the resonant discharge of the capacitor.

The turn-OFF processes of IGCTs have the greatest impact on the switching losses. The slower the voltage on the IGCT during the turn-OFF rises, the lower the losses are.

4. NUMERICAL ANALYSIS

4.1. The IGCT model

The IGCTs are manufactured for voltages of a few kV and currents of a few kA. So, it would not make sense to build a prototype of the 3LVSI with a rated power of a few MW without extensive prior research. Therefore, the switching losses and efficiency of the 3LVSI are analyzed using numerical simulations.

To analyze the operation and estimate losses in the 3LVSI, it is necessary to use an appropriate IGCT model. However, this cannot be a model that uses complex physical relations as presented in [30], because the 3LVSI contains 12 thyristors. Even in a relatively simple system using a model based on physical relations, problems with convergence of calculations occur, among other things. A model of the IGCT was proposed in [5], but its application for numerical calculations of various inverter operating states is difficult, e.g., no convergence of the solution, problems with entering catalog data of IGCTs. In numerical analysis, the model of the IGCT described in [34] was applied.

Since the IGCT is a modification of the Gate Turn-OFF Thyristor (GTO), the IGCT model is based on two GTOs connected in parallel (Fig. 10). Each GTO is represented by a two-transistor PNP-NPN system, and controlled by a SiC power MOSFET. A detailed description of this model is presented in [34]. In the presented model, the IGCT is turned ON by a positive gate current pulse and turned OFF by a negative gate current pulse. The model parameters were modified with respect to the values given in [34] to better reflect changes in the IGCT voltage and current during the turn-OFF process (Tables 2, 3 and 4).

It is worth noting that using two GTOs connected in parallel improves the calculation accuracy of changes in both the voltage and current during switching processes with respect to real waveforms. The authors of paper [34] emphasized that increasing the number of GTOs did not significantly improve the accuracy of numerical calculations.

The correctness of the IGCT model was verified by comparing the calculated waveforms with the waveforms recorded in laboratory test systems. Thanks to the courtesy and consent of the authors of paper [7], the voltage and current waveforms of IGCT type 5SHY 35L4521 (Table 5) recorded in the test circuit during the turn-OFF process are used for comparison, which are marked in Fig. 11 using continuous lines. The analogous changes in both the voltage and current determined with the use of the IGCT model are shown using dashed lines. The turn-OFF process of the considered IGCT was performed at a supply voltage of 5500 V and a current of 3300 A.

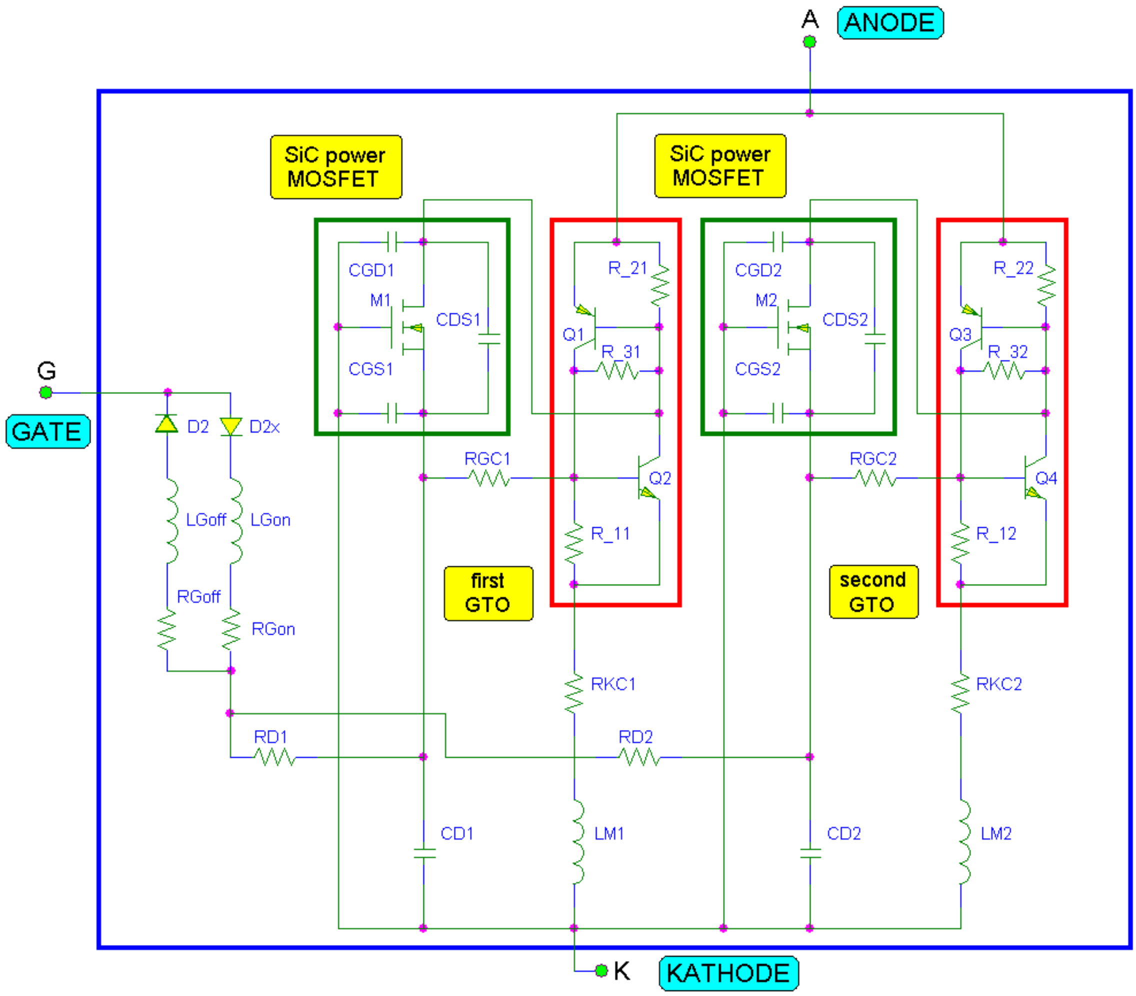

Fig. 10. The IGCT model

Table 2
Parameters of transistors Q1, Q2, Q3 and Q4 of GTO model

Model parameter	Notation	Q1, Q3	Q2, Q4
Transport saturation current	Is (pA)	1	1p
Ideal maximum forward beta	BF (–)	2	10
Ideal maximum reverse beta	BR (–)	1	1
Base-emitter leakage emission coefficient	NE (–)	2	2
Base-collector leakage saturation current	ISC (A)	1.5	1.5
Forward current emission coefficient	NF (–)	1	1
Base-collector leakage emission coefficient	NC (–)	0.1	0.1
Base-collector zero-bias p-n capacitance	CJC (nF)	0.6	0.6
Base-emitter zero-bias p-n capacitance	CJE (nF)	0.7	1.0
Ideal forward transit time	TF (μs)	1	2
Ideal reverse transit time	TR (μs)	1	2
Quasi-saturation temperature coefficient for hole mobility	CN (–)	2.20	2.42
Quasi-saturation temperature	D (–)	0.52	0.87

Table 3
Parameters of SiC power MOSFETs

Parameter	Notation	M1, M2
Channel length	L (μm)	100
Channel width	W (μm)	100
Pinch-off voltage	VTO (V)	5.61
Transconductance coefficient	KP (A/V)	28.04
Surface potential	PHI (V)	0.6
Source ohmic resistance	RS (Ω)	1.2
Bulk p-n saturation current	IS (pA)	10
Bulk p-n bottom potential	PB (V)	0.8
Bulk p-n sidewall potential	PBSW (V)	0.8
Mobility degradation critical field	UCRIT (kV/cm)	10
Capacitors of SiC power	MOSFETs (nF)	1

Table 4
Other parameters of IGCT model

RGon (mΩ)	LGon (μH)	RGoff (mΩ)	LGoff (nH)	RD1,2 (μΩ)	CD1,2 (nF)	LM1,2 (nH)	RKC1,2 (μΩ)
3	0.2	2	1	1	1	68	0.7

Table 5
Parameters of IGCT type 5SHY 35L4521

V_{DRM} (V)	$I_{T(AV)}$ (A)	$I_{T(RMS)}$ (A)	I_{TGQM} (A)	V_{TM} (V)	di/dt (A/μs)	E_{ON} (J)	E_{OFF} (J)
4500	1700	2670	4000	2.35	1000	1.5	19.5

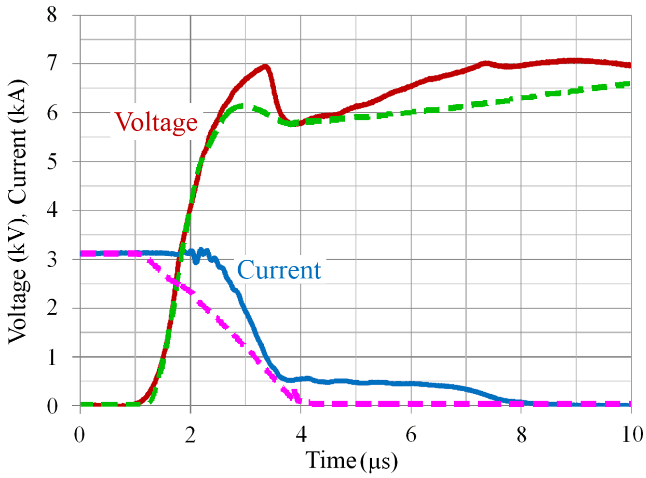

Fig. 11. Voltage and current waveforms during turn-OFF process. Measured waveforms are reproduced with permission from *U*. Vemulapati, in Proceedings of the 17-th European Conference on Power Electronics and Applications (EPE'15 ECCE-Europe), Geneva, Switzerland, 08–10 September; 2015

4.2. 10-MW inverter with soft-switching technique

The described soft-switching system is recommended for high-rated-power 3LVSIs. Therefore, the analysis of the system operation was conducted for a 10-MW inverter based on IGCT type CAC 3000-60 (Table 6).

Table 6
Parameters of IGCT type CAC 3000-60

V_{DRM} (V)	$I_{T(AV)}$ (A)	$I_{T(RMS)}$ (A)	I_{TGQM} (A)	V_{TM} (V)	di/dt (A/μs)	E_{ON} (J)	E_{OFF} (J)
6000	1300	2000	3000	3.0	1000	1.0	16.5

In the soft-switching system, fast thyristors type TFI773-1600-28 (1600 A, 2800 V) and fast recovery diodes type 5SDF 20L4520 (4500 V, 1970 A) were applied. It was assumed that air inductors were used in the soft-switching system. The losses in the inductors can be significantly reduced by using inductors with ferrite cores and an air gap; this allows the number of turns of the inductors to be reduced. The flux density of ferrites is most often no higher than about 0.3 T, and the coercive force is on average 20 A/m. Notably, the current in inductors flows only in one direction. Therefore, changes in both the field strength and flux density occur only in the first quarter of the ferrite hysteresis loop. Assuming that the maximum current of the inductors is about 3 kA, the power losses in the ferrite cores of all inductors are approximately 0.68 kW for the switching frequency of 1 kHz. These losses are approximately 1.35 kW and 2.03 kW for 2 kHz and 3 kHz, respectively.

The power losses P_{cap} of any capacitor can be calculated as follows

$$P_{cap} = \sum_{i=1}^{n} 2\pi f_i C V_{rmsi}^2 \tan\delta(f_i), \tag{16}$$

where f_i, V_{rmsi} and $\tan\delta$ denote the frequency, rms voltage and dissipation factor at the frequency of the i-th harmonic, respectively.

The dissipation factor $\tan\delta$ depends on the so-called equivalent series resistance ESR

$$\tan\delta = 2\pi f C ESR. \tag{17}$$

The ESR values for frequencies 1 kHz, 2 kHz and 3 kHz are approximately 0.98 mΩ, 0.57 mΩ and 0.43 mΩ, respectively. Parameters of the reactive components are presented in Table 7.

Table 7
Parameters of capacitors and inductors for $V_{DC} = 2500$ V, $I_{L\max} = 3000$ A, $t_{off} = 4$ µs

C11,14 (µF)	L11,14 (µH)	R11,14 (mΩ)	L11a,14a (µH)	R11a,14a (mΩ)	L12,13 (µH)	R12,13 (mΩ)
48.0	33.0	1.2	77.0	1.9	1.0	0.15

The squirrel-cage induction motor type AMI 630L2L B (P_N = 8 MW, $V_N = 3000$ V, $I_N = 1720$ A, $\cos\varphi_N = 0.92$, $\eta_N = 97.5\%$) was assumed as a load. Numerical analysis was performed for three switching frequencies.

Figure 12 shows waveforms of selected voltages and currents during a single inverter operation cycle when thyristor T11 is switched. A positive pulse G_{T11} on the gate of the main thyristor T11 is the turn-ON pulse. The negative pulse turns OFF the IGCT, and the maximum value of this current pulse is often greater than the rated current of the IGCT. Only the turn-ON pulse G_{T11a} is applied to the auxiliary fast thyristor T11a because this thyristor turns OFF itself. The current in thyristor T11 does not abruptly decrease to zero during the turn-OFF process, as this process takes several microseconds, unlike the turn-OFF of IGBTs, which takes significantly less than 1 microsecond.

Figure 13 presents selected waveforms in the 3LVSI with the soft-switching system and the load voltages and currents for two periods of the output voltage. The voltage across T11 during its switching interval is equal to zero if the thyristor T11 is turned ON, or equal to VDC when it is turned OFF, or reaches the $V_{C\max}$ value at the end of the turn-OFF process. Due to the cyclic charging and discharging of capacitor C11, its current is alternating.

Notably, the resonance processes related to the soft turn-OFF of the thyristor T11 do not affect the shape of the load voltage.

During the entire operating period, IGCTs T12 and T13 are also switched, but their switching processes occur at relatively low current values. Therefore, the turn-OFF losses are much smaller than those in thyristors T11 and T14.

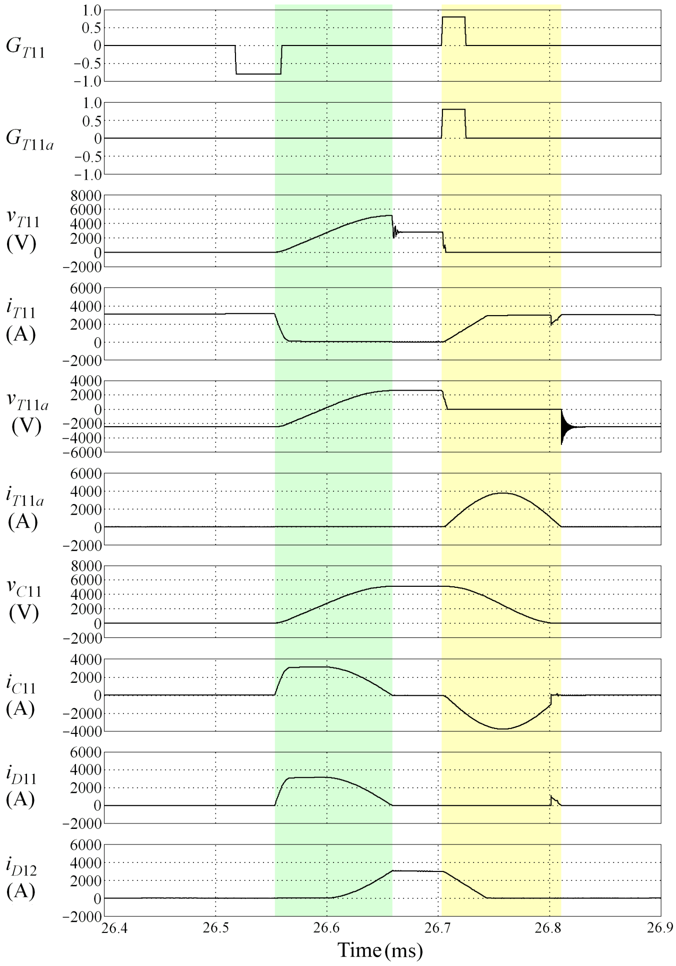

Fig. 12. Selected voltage and current waveform during single operation cycle; markings of waveforms according to Fig. 4; V_{DC} = 2500 V; switching frequency – 2 kHz; output frequency – 50 Hz; modulation depth factor – 0.82; I_{tr} = 30 A; green and yellow colors – processes related to the turn-OFF and turn-ON of IGCT, respectively

5. ESTIMATION OF POWER LOSSES

The efficiency of the 3LVSI with the hard-switching technique was estimated numerically in several articles, and it is averaged around 99.2% [2, 24, 35–37]. However, it should be emphasized that efficiencies were estimated at switching frequencies below 1 kHz. Even in this case, the switching losses in IGCTs and the turn-OFF losses in diodes are higher than the conduction losses in these components [24, 38]. For example, the switching losses in IGCTs and diodes in converters recommended for HVDC systems are approximately 66% of the total losses. The conduction losses in IGCTs and diodes change slightly with increasing frequency.

It was estimated in papers [23, 25] that IGCTs can currently operate at switching frequencies of up to 4–5 kHz. Therefore, the power losses and efficiency of the 3LVSI with the soft-switching system were estimated for three switching frequencies: 1 kHz, 2 kHz, and 3 kHz. The efficiency of the 3LVSI with the proposed soft-switching system was compared with the efficiency of the inverter with the hard-switching technique. The total losses were estimated using the PSpice software.

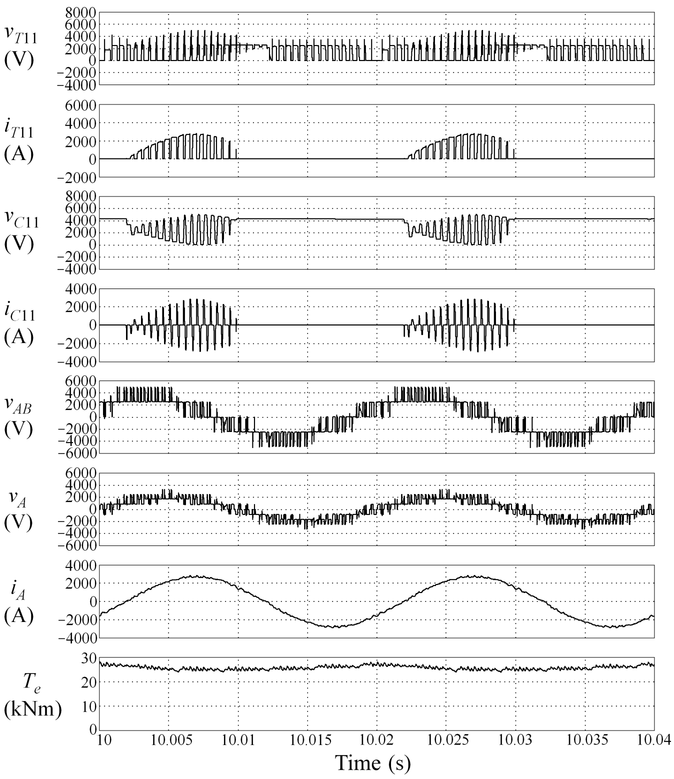

Fig. 13. Voltage and current waveforms in two periods of the output voltage; v_{AB}, v_A – phase-to-phase and phase voltage, respectively; i_A – load phase current, T_e – electromagnetic torque of a squirrel-cage induction motor; switching frequency – 2 kHz; output frequency – 50 Hz

Due to the complex shape of both the current and voltage waveforms during the turn-OFF process, useful analytical relationships determining power losses in IGCTs were not formulated. Therefore, the power losses were calculated as an integral of the product of the instantaneous voltage and current values of the particular elements. The losses during turn-ON processes are several times smaller than the losses during turn-OFF of the IGCTs, and they do not have a significant impact on the inverter efficiency.

The conduction losses also occur in auxiliary fast thyristors. However, all diodes of the 3LVSI with the soft-switching technique turn OFF softly. The values of individual losses for the three switching frequencies are presented in Table 8. Note that the conduction losses also occur in auxiliary fast thyristors. The efficiencies as a function of the load power are shown in Figs. 14 and 15.

The increase in the efficiency of the 3LVSI with the soft-switching system compared to the efficiency of the inverter with the hard-switching technique is relatively small at the frequency of 1 kHz. In this case, using the soft-switching technique may not produce the expected results. The efficiency increase of the 3LVSI with the soft-switching technique is approximately 0.4% at a frequency of 1 kHz, 1% at a frequency of 2 kHz and approximately 1.6% at frequency of 3 kHz. It is significant at rated power of several or more than a dozen MW. The efficiency of the 3LVSI with the proposed soft-switching system also depends on the parameter k (see Figs. 14 and 15). The results presented in Table 8 are partially displayed in Figs. 16 and 17.

The switching method of the IGCTs according to the algorithm shown in Fig. 3 leads to a reduction in the efficiency of the 3LVSI with the soft-switching system by approximately 0.39%,

Table 8
Comparison of power losses in 3LVSIs (in kW)

1 kHz		2 kHz		3 kHz	
Soft	Hard	Soft	Hard	Soft	Hard
Switching and conduction losses in T11 and T12					
Switching losses in T11					
1.43	7.43	2.77	14.95	4.37	22.43
Switching losses in T12					
0.16	0.40	0.53	0.73	0.45	0.92
Conduction losses in T11					
1.32	1.44	1.23	1.44	1.27	1.43
Conduction losses in T12					
2.38	2.38	2.38	2.37	2.27	2.36
Individual losses in 3LVSI					
Switching losses in the main thyristors					
9.52	46.98	19.80	94.07	28.88	140.07
Conduction losses in the main thyristors					
22.19	22.92	21.66	22.84	21.25	22.77
Turn-OFF losses in the diodes (only in hard-switching 3LVSI)					
–	1.34	–	3.10	–	4.78
Conduction losses in the diodes					
18.88	7.90	18.08	7.83	14.96	7.74
Turn-ON losses in the auxiliary thyristors					
0.39	–	0.71	–	0.98	–
Conduction losses in the auxiliary thyristors					
0.80	–	1.70	–	2.49	–
Conduction losses in the inductors					
12.32	–	15.60	–	18.71	–
Conduction losses in the resonant capacitor					
0.81	–	1.21	–	1.65	–
Power losses in the snubbers					
2.863	20.19	7.073	36.99	7.962	53.35
Total power losses and efficiency of 3LVSI					
Total power losses in the inverter					
67.78	99.32	85.84	164.80	96.88	228.70
Efficiency (%)					
99.16	98.77	98.94	97.98	98.80	97.22

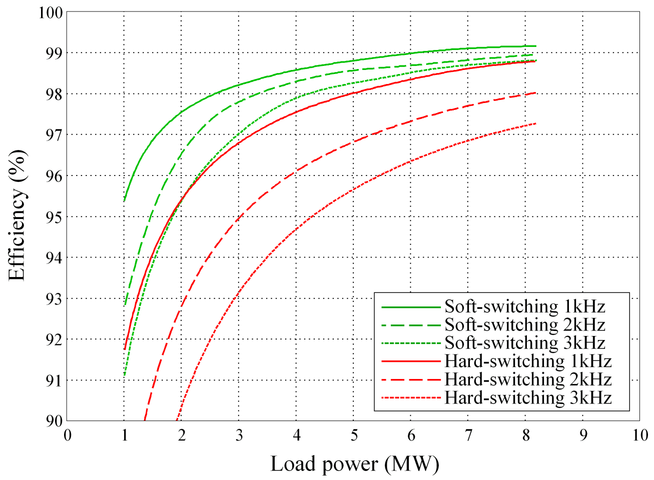

Fig. 14. Efficiency of 10-MW inverter for $k = 2.0$ as a function of the load power for three switching frequencies and for 3LVSI: green lines – inverter with soft-switching system; red lines – inverter with hard-switching technique; continuous, dashed, and dotted lines – switching frequency 1 kHz, 2 kHz, and 3 kHz, respectively

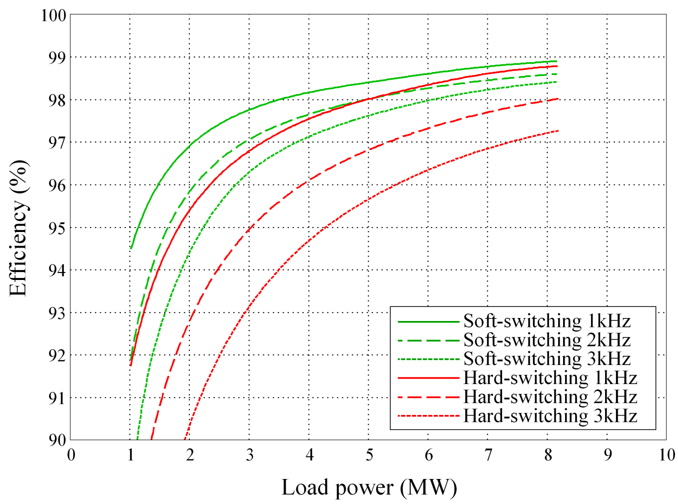

Fig. 15. Efficiency of 10-MW inverter for $k = 1.5$ as function of the load power for three switching frequencies: markings as in Fig. 14

0.96% and 1.58% for $k = 2$ and switching frequencies of 1 kHz, 2 kHz, and 3 kHz, respectively.

Note that capacitor losses should be considered in a more detailed analysis. These losses depend on factors such as equivalent series resistance (ESR), assumed value of the V_{Coff}, charging and discharging time, etc. Due to the varying load current, these losses vary for each switching cycle. Additionally, capacitor currents are not sinusoidal, which may cause certain difficulties in formulating the appropriate capacitor model. The power losses in the capacitors depend significantly on the switching frequency.

To compare the switching techniques, the total harmonic distortion (THD) of the load current was estimated for both the soft- and hard-switching techniques (Table 9).

The results of the numerical analysis indicate that the slight increase in the THD factor in the 3LVSI with the soft-switching system is caused by the interaction of the resonance processes related to the IGCT turn-OFF processes.

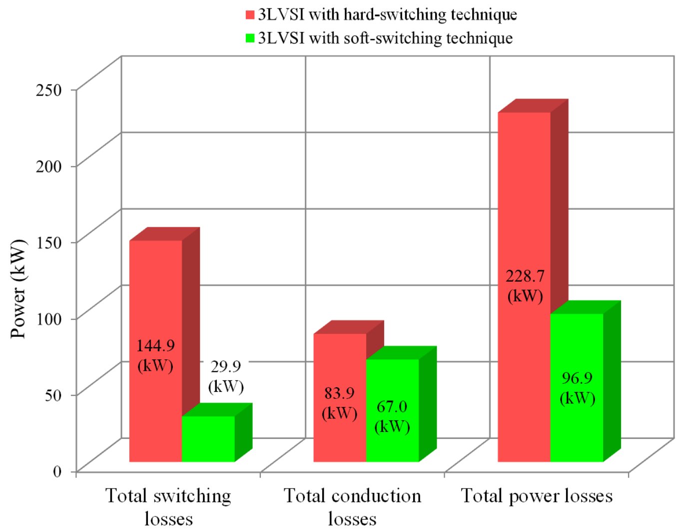

Fig. 16. Comparison of losses; switching frequency: 3 kHz, $k = 2.0$

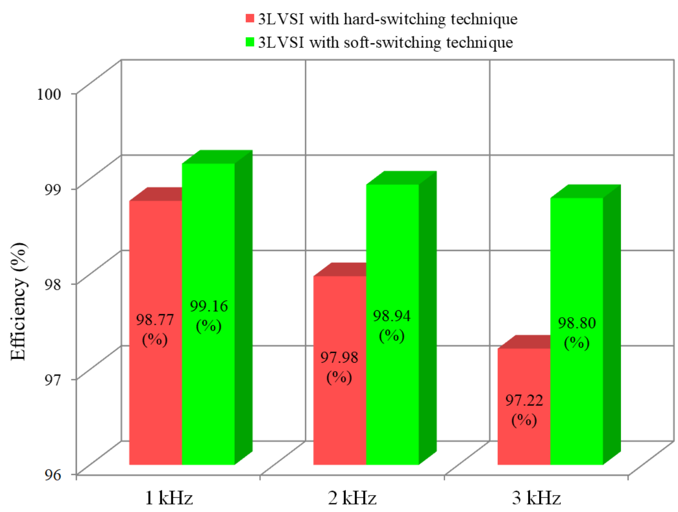

Fig. 17. Efficiencies for 10-MW 3LVSI for $k = 2.0$

Table 9
THD in % of the phase load current for rated load power at $k = 2.0$

Switching frequency	1 kHz	2 kHz	3 kHz
Hard-switching	3.08	1.50	0.99
Soft-switching	3.26	1.92	1.21

6. CONCLUSIONS

In the proposed soft-switching system in the three-phase 3LVSI, the voltage across the IGCTs, connected to the voltage source terminals, increases slowly during the turn-OFF processes. As a result, the turn-OFF losses are much smaller than in the inverter with the hard-switching technique. The use of the soft-switching technique allows for reducing power losses by several dozen or even several hundred kW, depending on the rated power of the inverter.

The capacitors are not connected in parallel to the main thyristors; therefore, it is not possible to discharge them through the conducted main IGCT. The inductors that limit the current of the resonant capacitor discharge are connected in series with the fast thyristors, which turn themselves OFF when their current is reduced to zero. Therefore, there is no risk of a sudden interruption of the current flowing through these inductors. It is worth emphasizing that the auxiliary fast thyristors are turned ON simultaneously with the corresponding main IGCTs; this makes the control system relatively simple.

The turn-OFF processes of IGCTs that are connected to voltage source terminals are soft; this leads to a significant reduction in total power losses. Consequently, the efficiency of the three-phase three-level voltage source inverter is higher than the efficiency of the inverter operating with the hard-switching technique.

It is worth noting that no proposals for soft switching in the 3LVSIs based on the IGCTs are in the available literature. Therefore, the suggestion presented to reduce the turn-OFF losses in the IGCTs can be regarded as a basis for further research.

REFERENCES

[1] B. Backlund, M. Rahimo, S. Klaka, and J. Siefken, "Topologies, voltage ratings and state of the art high power semiconductor devices for medium voltage wind energy conversion," in *Proc. IEEE Power Electronics and Machines in Wind Appl.*, 2009, pp. 24–26, doi: 10.1109/PEMWA.2009.5208365.

[2] C. Wang, C. Li, Y. Li, C. Zhu, and Z. Lan, "Large power three-level voltage source inverter with IGCTs and the experiment," in *Proc. IEEE Energy Conversion Congress and Exposition*, 2010, pp. 2087–2090, doi: 10.1109/ECCE.2010.5618244.

[3] L. Zhiming, L. Chongjian, L. Yaohua, Z. Chunyi, W. Chengsheng, and Y. Qiongtao, "Investigation on the 30MVA IGCT-Based Voltage Source Converter," in *Proc. 15th International Power Electronics and Motion Control Conf.* (EPE/PEMC), 2012, pp. DS1b.19-1–19-4, doi: 10.1109/EPEPEMC.2012.6397219.

[4] Z. Lan, Y. Li, C. Li, C. Zhu, and C. Wang, "Investigation on IGCT-Based NPC/H-Bridge Large Power Converter," in *Proc. IEEE Energy Conversion Congress and Exposition* (ECCE), 2012, pp. 726–730, doi: 10.1109/ECCE.2012.6342748.

[5] G. Lyu, C. Zhuan, R. Zeng, T. Long, and P. Palmer, "Physics-based Compact Model of Integrated Gate-Commutated Thyristor with Multiple Effects for High Power Application," *IET Power Electron.*, vol. 11, no. 7, pp. 1239–1247, 2018, doi: 10.1049/iet-pel.2017.0863.

[6] M. Rahimo, M. Arnold, U. Vemulapati, and T. Stiasny, "Optimization of High Voltage IGCTs towards 1V On-State Losses," in *Proc. PCIM Europe; International Exhibition and Conference for Power Electronics, Intelligent Motion, Renewable Energy and Energy Management*, 2013, pp. 1–8. [Online]. Available: https://www.academia.edu/76035156/Optimization_of_High_Voltage_IGCTs_towards_1V_On_State_Losses.

[7] U. Vemulapati, M. Rahimo, M. Arnold, T. Wikström, J. Vobecky, and B. Backlund, "Recent Advancements in IGCT Technologies for High Power Electronics Applications," in *Proc. 17th European Conference on Power Electronics and Applications* (EPE'15 ECCE-Europe), 2015, pp. 08–10, doi: 10.1109/EPE.2015.7311740.

[8] D. Stamenkovic, D. Dujic, M. Rahimo, U. Vemulapati, and T. Stiasny, "IGCT Switching Behaviour Under Resonant Operating Conditions," in *Proc. 20th European Conference on Power Electronics and Applications* (EPE'18 ECCE Europe), 2018, pp. P.1–P.9. [Online]. Available: https://ieeexplore.ieee.org/abstract/document/8515650.

[9] D. Stamenkovic, U. Vemulapati, M. Rahimo, T. Stiasny, and D. Dujic, "IGCT Switching Behaviour Under Low Current Conditions," in *Proc. PCIM Europe; International Exhibition and Conference for Power Electronics, Intelligent Motion, Renewable Energy and Energy Management*, 2018, pp. 777–782. [Online]. Available: https://ieeexplore.ieee.org/document/8402927.

[10] Z. Chen, Z. Yu, X. Liu, J. Liu, and R. Zeng, "Stray Impedance Measurement and Improvement of High-Power IGCT Gate Driver Units," *IEEE Trans. Power Electron.*, vol. 34, no. 7, pp. 6639–6647, 2019, doi: 10.1109/TPEL.2018.2826046.

[11] D. Stamenkovic and D. Dujic, "Application of the IGCT for Resonant Conversion with Low Switching losses," *IEEJ J. Ind. Appl.*, vol. 9, no. 3, pp. 244–253, 2020, doi: 10.1541/ieejjia.9.244.

[12] D. Stamenkovic, U. Vemulapati, T. Stiasny, M. Rahimo, and D. Dujic, "IGCT Low-Current Switching—TCAD and Experimental Characterization," *IEEE Trans. Ind. Electron.*, vol 67, no. 8, pp. 6302–6311, 2020, doi: 10.1109/TIE.2019.2939996.

[13] U. Vemulapati, D. Johannesson, T. Wikström, T. Stiasny, C. Corvace, and C. Winter, "High-Voltage (8.5 kV) Asymmetric IGCT for MVD and HVDC Applications," in *Proc. 11th International Conference on Power Electronics-ECCE Asia*, 2023, pp. 1189–1194, doi: 10.23919/ICPE2023-ECCEAsia54778.2023.10213487.

[14] P. Ladoux, N. Serbia, and E.I. Carroll, "On the Potential of IGCTs in HVDC," *IEEE J. Emerging Sel. Top. Power Electron.*, vol. 3, no. 3, pp. 780–793, 2015, doi: 10.1109/JESTPE.2015.2429116.

[15] Z. Chen, Z. Yu, X. Zhang, T. Wei, G. Lyu, and L. Qu, "Analysis and Experiments for IGBT, IEGT, and IGCT in Hybrid DC Circuit Breaker," *IEEE Trans. Ind. Electron.*, vol. 65, no. 4, pp. 2883–2892, 2018, doi: 10.1109/TIE.2017.2764863.

[16] L. Zhiming, L. Yaohua, L. Chongjian, W. Chengsheng, and D. Wei, "Investigation on 30MV A IGCT -based High Power Converter," in *Proc. 7th International Power Electronics and Motion Control Conf.*, 2012, pp. 1652–1655, doi: 10.1109/IPEMC.2012.6259082.

[17] S. Bhattacharya and S. Babaei, "Series Connected IGCT Based ThreeLevel Neutral Point Clamped Voltage Source Inverter Pole for High Power Converters," in *Proc. IEEE Energy Conversion Congress and Exposition*, 2011, pp. 4248–4255, doi: 10.1109/ECCE.2011.6064349.

[18] D. Andler, R. Álvarez, S. Bernet, and J. Rodríguez, "Experimental Investigation of the Commutations of a 3L-ANPC Phase Leg Using 4.5-kV–5.5-kA IGCTs," *IEEE Trans. Ind. Electron.*, vol. 60, no. 11, pp. 4820–4830, 2013, doi: 10.1109/TIE.2012.2227903.

[19] T. Thurnherr, P. Maibach, B. Buchmann, and E. Baerlocher, "Static Frequency Converters for Railway Power Supply based on IGCT High Power Semiconductors," in *Proc. International Exhibition and Conference for Power Electronics, Intelligent

Motion, Renewable Energy and Energy Management, 2020, pp. 334–341. [Online]. Available: https://ieeexplore.ieee.org/abstract/document/9178018.

[20] F. Agostini, U. Vemulapati, T. Torresin, M. Arnold, M. Rahimo, and A. Antoniazzi, "1MW Bi-directional DC Solid State Circuit Breaker based on Air Cooled Reverse Blocking-IGCT," in *Proc. IEEE Electric Ship Technologies Symp.* (ESTS), 2015, pp. 287–292, doi: 10.1109/ESTS.2015.7157906.

[21] R. Rodrigues, Y. Du, A. Antoniazzi, and P. Cairoli, "A Review of SolidState Circuit Breakers," *IEEE Trans. Ind. Electron.*, vol. 36, no. 1, pp. 364–377, 2021, doi: 10.1109/TPEL.2020.3003358.

[22] S. Shirmohammadi and Y. Suh, "Multi-winding Flyback Type Snubber for 10kV IGCT with Reduced Voltage Stress on Recovery Diodes," in *Proc. IEEE Energy Conversion Congress and Exposition* (ECCE), 2018, pp. 964–971, doi: 10.1109/ECCE.2018.8558290.

[23] D. Stamenkovic, U. Vemulapati, T. Stiasny, M Rahimo, and D. Dujic, "Soft Switching Behavior of IGCT for Resonant Conversion," in *Proc. IEEE Applied Power Electronics Conference and Exposition* (APEC), 2019, pp. 2714–2719, doi: 10.1109/APEC.2019.8722039.

[24] D. Guedon, P. Ladoux, S. Sanchez, and S. Cornet, "High Voltage IGCTs for HVDC Converter-Stations," in *Proc. AEIT HVDC International Conf.* (AEIT HVDC), 2021, doi: 10.1109/AEITHVDC52364.2021.9474610.

[25] Y. Ma *et al.*, "An IGCT-Series-Based DC Transformer With Quasi-Zero Switching Loss Modulation by Minimum Backflow Power Injection," *IEEE Trans. Power Electron.*, vol. 38, no. 12, pp. 15566–15578, 2023, doi: 10.1109/TPEL.2023.3306598.

[26] C. Xu, Z. Yu, B. Zhao, Z. Wang, Z. Chen, and R. Zeng, "Ultra-Low Reactive Power Operation and Control Strategy of Hybrid Line Commutated Converter Based on IGCT for HVdc Application," *IEEE Trans. Ind. Electron.*, vol 70, no. 12, pp. 12926–12932, 2023, doi: 10.1109/TIE.2023.3236116.

[27] W. Zhou *et al.*, "Comprehensive Analysis, Design, and Experiment of Shoot-Through Faults in MMC Based on IGCT for VSC-HVDC," *IEEE Trans. Power Electron.*, vol. 36, no. 6, pp. 6241–6250, 2021, doi: 10.1109/TPEL.2020.3034423.

[28] W. Zhou *et al.*, "Systematic Analysis and Characterization of Extreme Failure for IGCT in MMC-HVdc System – Part I: Device Structure, Explosion Characteristics, and Optimization," *IEEE Trans. Power Electron.*, vol. 37, no. 7, pp. 8076–8086, 2022, doi: 10.1109/TPEL.2022.3146273.

[29] G. Ulissi, J. Kucka, U. Vemulapati, T. Stiasny, and D. Dujic, "Resonant IGCT Soft-Switching: Zero-Voltage Switching or Zero-Current Switching," IEEE Trans. Power Electron., vol. 37, no. 9, pp. 10775–10783, 2022, doi: 10.1109/TPEL.2022.3170114.

[30] J. Wang, L. Chen, X. Zhang, J. Liu, B. Zhao, and Z. Yu, "Enhancing Turn-Off Performance in IGCT-Based High Power Applications – Part I: Anomalous High Current Turn-Off Mode and Safe Operating Area Expansion at Ultra-Low Voltage," *IEEE Trans. Power Electron.*, vol. 40, no. 4, pp. 5309–5318, 2025, doi: 10.1109/TPEL.2024.3508835.

[31] L. Chen *et al.*, "Enhancing Turn-Off Performance in IGCT-Based High Power Applications – Part II: Hybrid Switch With IGBT Integration and Experimental Validation," *IEEE Trans. Power Electron.*, vol. 40, no. 2, pp. 3168–3176, 2025, doi: 10.1109/TPEL.2024.3481967.

[32] W. Mazgaj and Z. Szular, "The system and method for the softswitching of turn-off thyristors connected to the terminals of a DC voltage source supplying a three-phase, three-level voltage source inverter," Patent application no. P.451112, Poland.

[33] Z. Szular, B. Rozegnal, and W. Mazgaj, "A new Soft-Switching Solution in Three-Level Neutral-Point-Clamped Voltage Source Inverter," *Energies*, vol. 14, 2021, doi: 10.3390/en14082247.

[34] Y. Song, C. Wang, W. Yang, and J. Yang, "IGCT Circuit Model Based on Pspice Modeling Platform," in *Proc. 1st Workshop on Wide Bandgap Power Devices and Applications in Asia* (WiPDA Asia), 2018, pp. 114–117, doi: 10.1109/WiPDAAsia.2018.8734669.

[35] L. Ceccarelli, F. Iannuzzo, and M. Nawaz, "PSpice modeling platform for SiC power MOSFET modules with extensive experimental validation," in *Proc. IEEE Energy Conversion Congress and Exposition* (ECCE), 2016, doi: 10.1109/ECCE.2016.7855369.

[36] A.V. Rocha1, G.J. França, M.E. Santos, H. Paula, and B.J. Cardoso Filho, "A fault-resilient implementation of three level NPC IGCT-based converters," *Eletrôn. Potên., Campo Grande*, vol. 16, no. 2, pp. 168–176, 2011, doi: 10.18618/REP.2011.2.168176.

[37] A.L. Lyngdoh, Y. Suh, B.G. Park, and J. Kim, "Thermal Performance Analysis of 10kV IGCT based Three Level ANPC Converter in 7MW PMSG MV Wind Turbines," in *Proc. 10th International Conference on Power Electronics and ECCE Asia* (ICPE 2019 — ECCE Asia), 2019, doi: 10.23919/ICPE2019-ECCEAsia42246.2019.8796982.

[38] B. Zhao *et al.*, "Practical Analytical Model and Comprehensive Comparison of Power Loss Performance for Various MMCs Based on IGCT in HVDC Application," *IEEE J. Emerging Sel. Top. Power Electron.*, vol. 7, no. 2, pp. 1071–1083, 2019, doi: 10.1109/JESTPE.2018.2871191.